Inorg. Chem. **XXXX**, *XX*,

Inorganic Chemistry
Article

Supramolecular Architectures and Magnetic Properties of Coordination Polymers Based on Pyrazinedicarboxylato Ligands Showing Embedded Water Clusters

Garikoitz Beobide, Oscar Castillo,* Antonio Luque, Urko García-Couceiro, Juan P. García-Terán, and Pascual Román

Departamento de Química Inorgánica, Facultad de Ciencia y Tecnología, Universidad del País Vasco/Euskal Herriko Unibertsitatea, Apartado 644, E-48080 Bilbao, Spain

Received February 8, 2006

The synthesis, crystal structure, and magnetic behavior of nine transition-metal complexes based on pyrazine-2,5-dicarboxylato (*pz25dc*) and pyrazine-2,3-dicarboxylato (*pz23dc*) ligands are reported. The *pz25dc* ligand displays a bis-bidentate coordination mode, with the carboxylate groups almost coplanar with the pyrazine ring, to afford polymeric 1-D chains [Mn(**1**), Fe(**2**), Zn(**3**), and Cu(**4** and **5**)] and discrete dimeric entities [Mn(**6**)] when the 1,10-phenanthroline (*phen*) blocking ligand is used to avoid further polymerization. The nonplanar *pz23dc* ligand chelates to a unique copper center, while it bridges another one or two metal centers via the remaining carboxylate group, leading to 1-D polymeric chains (**7**), ladder chains (**8**), and sheets (**9**). The crystal packing of the metal-organic frameworks of compounds **4**–**9** generates voids which are occupied by assembled water molecules. The different water cluster patterns (tapes, four-membered discrete rings, and chains for compounds **6**, **8**, and **9**, respectively) and their role in the cohesiveness of supramolecular architectures are analyzed. Thermogravimetric and variable-temperature X-ray powder diffraction studies have revealed the occurrence of reversible dehydration processes in compounds **6**, **8**, and **9**. Furthermore, the magnetic behavior of these compounds has been studied in order to analyze the capability of the pyrazine ring to transmit magnetic interactions.

Introduction

In recent years, the area of inorganic crystal engineering[1] has become one of intense research activity because of the growing need for novel solid-state architectures with potential applications as functional materials in fields such as catalysis, conductivity, zeolitic behavior, and magnetism.[2] The judicious choice of the metal ion, a good understanding of the coordination preferences of the bridging entities, and a careful selection of the terminal ligands are key steps for the rational design of metal-organic coordination polymers with novel topologies and specific chemical and physical properties.[3] In this context, π-conjugated N-donor bridging ligands, such as pyrazine and its polycarboxylic derivatives, have appeared to be well-suited tools for the construction of extended arrays of metal ions with interesting physical properties in molecular magnetism or selective guest adsorption fields.[4,5] Among them, the synthesis and characterization of metal coordination polymers based on the pyrazine-2,3-dicarboxylato (*pz23dc*) ligand has evolved rather rapidly in recent years,[5,6] mostly because of two reasons: (a) the presence of two carboxylate

* To whom correspondence should be addressed. Phone: 34 946-015-991. Fax: 34 944-013-500. E-mail: oscar.castillo@ehu.es.

(1) (a) Brammer, L. *Chem. Soc. Rev.* **2004**, *33*, 476−489. (b) Braga, D.; Brammer, L.; Champness, N. R. *CrystEngComm.* **2005**, *7*, 1−19.

(2) (a) James, S. L. *Chem. Soc. Rev.* **2003**, *32*, 276−288. (b) Janiak, C. *J. Chem. Soc., Dalton Trans.* **2003**, 2781−2804.

(3) (a) Holliday, B. J.; Mirkin, C. A. *Angew. Chem., Int. Ed.* **2001**, *40*, 2022−2043. (b) Braga, D.; Desiraju, G. R.; Miller, J. S.; Orpen, A. G.; Price, S. L. *CrystEngComm.* **2002**, *4*, 500−509.

(4) (a) O'Connor, C. J.; Klein, C. L.; Majeste, R. J.; Trefonas, L. M. *Inorg. Chem.* **1982**, *21*, 64−67.

(5) (a) Kondo, M.; Okubo, T.; Asami, A.; Noro, S. I.; Yoshitomi, T.; Kitagawa, S.; Ishii, T.; Matsuzaka, H.; Seki, K. *Angew. Chem., Int. Ed.* **1999**, *38*, 140−143. (b) Kitaura, R.; Fujimoto, K.; Noro, S.; Kondo, M.; Kitagawa, S. *Angew. Chem., Int. Ed.* **2002**, *41*, 133−135. (c) Li, D.; Kaneko, K. *J. Phys. Chem. B* **2000**, *104*, 8940−8945. (d) Maji, T. K.; Uemura, K.; Chang, H.-C.; Matsuda, R.; Kitagawa, S. *Angew. Chem., Int. Ed.* **2004**, *43*, 3269−3272.

(6) (a) Gryz, M.; Starosta, W.; Ptasiewciz-Bak, H.; Leciejewicz, J. *J. Coord. Chem.* **2003**, *56*, 1575−1579. (b) Konar, S.; Manna, S. C.; Zangrando, E.; Chaudhuri, N. R. *Inorg. Chim. Acta* **2004**, *357*, 1593−1597. (c) Premkumar, T.; Govindarajan, S. *Inorg. Chem. Commun.* **2003**, *6*, 1385−1389. (d) Zou, J.-Z.; Xu, Z.; Chen, W.; Lo, K. M.; You, X.-Z. *Polyhedron* **1999**, *18*, 1507−1512. (e) Liang, Y.; Hong, M.; Cao, R.; Su, W.; Zhao, Y.; Weng, J.; Xiong, R. *Bull. Chem. Soc. Jpn.* **2002**, *75*, 1521−1526.

10.1021/ic060221r CCC: $33.50

Published on Web 06/07/2006

groups as substituents in the N-heterocyclic pyrazine ring allows multiple coordination modes, and (b) the steric hindrance between these groups leads to the noncoplanarity of the carboxylate groups (donor O atoms) and the pyrazine ring (donor N atoms), which aids to increase the dimensionality of the assembled covalent networks. The pyrazine-2,5-dicarboxylate anion (*pz25dc*) does not present the above cited steric hindrance, and as a consequence, both groups are nearly coplanar with the pyrazine ring.[7] The properties and coordination features of metal complexes based on *pz25dc* have been much less investigated. Nowadays, as far as we are aware, two polymeric manganese and strontium complexes[8] and two discrete binuclear complexes of copper[9] and vanadium[10] are the only structurally characterized examples containing a metal and this ligand as either a bridging or terminal group. In the first one, the ligand bridges simultaneously four Mn(II) atoms in a hexadentate way, while in the latter compounds, the *pz25dc* ligand acts as bis-bidentate bridge between two Cu(II) or V(V) atoms. Because of the structural features of *pz25dc*, the bis-bidentate coordination mode could be expected for many transition-metal complexes. This fact allows the *pz25dc* ligand to be a suitable molecule for the straightforward design and construction of polynuclear complexes. Moreover, in the area of molecular magnetism, a lot of work has been devoted to the study of the magnetic coupling between two paramagnetic centers bridged by a diazine ligand,[11] and this ligand is well-suited to conduct this kind of study. The nature and magnitude of the coupling constant can vary substantially depending on factors such as the nature of the paramagnetic center, the topology of the bridging ligand, or the influence of the terminal ligands. A better understanding of the magnetic interactions and magneto-structural relationships in these kinds of metal complexes can be achieved by means of spin delocalization and polarization concepts.[12]

As a part of an extended study concerning the use of substituted diazine rings ($C_4H_2N_2$) on the design and construction of polynuclear metal complexes,[8a,9] here, we report the synthesis, crystal structure, and magnetic properties of nine novel transition-metal complexes based on the *pz*2*5dc* and *pz*2*3dc* ligands in which the selection of the proper chemical factors has allowed us to control the dimensionality of the covalent skeleton. A common feature of these kinds of metal-organic frameworks (MOFs) is the high trend to present embedded water clusters when additional terminal ligands are present. These crystallization water molecules can present as isolated ones tightly H-bonded to the MOF or as aggregates which fill the empty voids or channels generated in the crystal packing. The release of the water molecules, in the latter case, can lead to the formation of porous anhydrous compounds with several potential applications in areas such as chemical separation, catalysis, and sorption. In fact, the study of the gas adsorption capability of the dehydrated products of several *pz23dc* metal complexes has become of great interest in the past few years.[5] These studies have revealed the formation of ordered arrays of adsorbed gas molecules within the voids previously occupied by the water molecules.[13] Moreover, oligomeric and polymeric arrays of water molecules have been extensively studied both theoretically and experimentally as they can provide not only insights into the supramolecular architecture[14] or water-condensed phase properties[15] but also clues on many biological processes.[16] For example, water chains appear to be important in the control of proton translocation through membranes by functioning as proton wires,[17] and a close behavior has been observed in the solid-state hydrated phase of an abiological imidazole derivative.[18] Because it is impossible for water clusters in solution and in the solid state to be fully discrete, the precise structural data and cooperative association of the water clusters and crystal hosts may be helpful in improving our understanding of the contribution of water clusters to the stability and function of the biological assemblies, as well as anomalous properties of water.

Experimental Section

Chemicals. All chemicals were of reagent grade and were used as commercially obtained. Standard literature procedures were used to prepare the starting material $K_2[Cu(pz23dc)_2(H_2O)]\cdot 6H_2O$.[19]

Synthesis of $[M(\mu\text{-}pz25dc)(H_2O)_2]_n$ [M(II) = Mn(1), Fe(2), Zn(3)]. An aqueous solution (10 mL) of $Mn(NO_3)_2\cdot 4H_2O$ (0.0753 g, 0.3 mmol), $FeCl_2\cdot 4H_2O$ (0.0596 g, 0.3 mmol), or $ZnCl_2$ (0.0409 g, 0.3 mmol) was added dropwise to a solution (water 10 mL) of $H_2pz25dc\cdot 2H_2O$ (0.612 g, 0.3 mmol) basified to pH = 5 using a KOH aqueous solution. Immediately, a polycrystalline powder

(7) (a) Harlow, L. R.; Simonsen, S. H. *Acta Crystallogr., Sect. B* **1974**, *30*, 1370−1372. (b) Ptasiewicz-Bak, H.; Leciejewicz, J. *J. Coord. Chem.* **1998**, *44*, 299−309.

(8) (a) Beobide, G.; Castillo, O.; Luque, A.; García-Couceiro, U.; García-Terán, J. P.; Román, P. *Inorg. Chem. Commun.* **2003**, *6*, 1224−1227. (b) Xu, H. T.; Zheng, N. W.; Yang, R. Y.; Li, Z. Q.; Jin, X. J. *Inorg. Chim. Acta* **2003**, *349*, 265−268. (c) Ptasiewicz-Bak, H.; Leciejewicz, J. *J. Coord. Chem.* **1998**, *44*, 237−246.

(9) Beobide, G.; Castillo, O.; García-Couceiro, U.; García-Terán, J. P.; Luque, A.; Martínez-Ripoll, M.; Román, P. *Eur. J. Inorg. Chem.* **2005**, 2586−2589.

(10) Süss-Fink, G.; Gonzalez-Cuervo, L.; Therrien, B.; Stoeckli-Evans, H.; Shul'pin, G. B. *Inorg. Chim. Acta* **2004**, *357*, 475−484.

(11) Manson, J. L.; Schueleter, J. A.; Koo, H. J.; Whangbo, M. H. *Inorg. Chem.* **2004**, *43*, 4007−4011.

(12) Cano, J.; Ruiz, E.; Alvarez, S.; Verdaguer, M. *Comments Inorg. Chem.* **1998**, *20*, 27−56.

(13) (a) Kitaura, R.; Kitagawa, S.; Kubota, Y.; Kobayashi, T. C.; Kindo, K.; Mita, Y.; Matsuo, A.; Kobayashi, M.; Chang, H. C.; Ozawa, T. C.; Suzuki, M.; Sakata, M.; Takata, M. *Science* **2002**, *298*, 2358−2361. (b) Kubota, Y.; Takata, M.; Matsuda, R.; Kitaura, R.; Kitagawa, S.; Kato, K.; Sakata, M.; Kobayashi, T. C. *Angew Chem., Int. Ed.* **2005**, *44*, 920−923. (c) Kitaura, R.; Matsuda, R.; Kubota, Y.; Kitagawa, S.; Takata, M.; Kobayashi, T. C.; Suzuki, M. *J. Phys. Chem. B* **2005**, *109*, 23378−23385.

(14) (a) Ghosh, S. K.; Bharadwaj, P. K. *Inorg. Chem.* **2004**, *43*, 6887−6889. (b) Edgar, M.; Mitchell, R.; Slawin, A. M. Z.; Lightfoot, P.; Wright, P. A. *Chem.—Eur. J.* **2001**, *7*, 5168−5175.

(15) (a) Ludwing, R. *Angew. Chem., Int. Ed.* **2003**, *42*, 3458−3460. (b) Keutsch, N. K.; Saykally, R. J. *J. Proc. Natl. Acad. Sci. U.S.A.* **2001**, *98*, 10533−10540.

(16) (a) ten Wolde, P. R.; Frenkel, D. *Science* **1997**, *277*, 1975−1978. (b) Pomès, R.; Roux, B. *Biophys. J.* **2002**, *82*, 2304−2316. (c) Cukierman, S. *Biophys. J.* **2000**, *78*, 1825−1834.

(17) Tieleman, D. P.; Biggin, P. C.; Smith, G. R.; Sansom, S. P. *Q. Rev. Biophys.* **2001**, *34*, 473−561.

(18) Cheruzel, L. E., Pometun, M. S.; Cecil, M. R.; Mashuta, M. S.; Witterbort, R. J.; Buchanan, R. M. *Angew. Chem., Int. Ed.* **2003**, *42*, 5452−5455.

(19) Castillo, O.; Beobide, G.; Luque, A.; Román, P. *Acta Crystallogr., Sect. E* **2003**, *59*, m800−m802.

corresponding to compounds **1** (yellow), **2** (navy blue), or **3** (white) appeared. The precipitate was separated from the mother liquor, washed with methanol and diethyl ether, and dried in the air. Yield: 85−90%. Compound **1**: Anal. Calcd for $C_6H_6MnN_2O_6$: C, 28.02; H, 2.35; N, 10.90; Mn, 21.38. Found: C, 28.11; H, 2.28; N, 11.02; Mn, 21.30. Main IR features (cm^{-1}, KBr pellet): 3250 vs for ν(O−H); 3091 w for ν(C−H); 1670 vs for [ν_{as}(O−C−O) + ν(C═C + C═N)]; 1479 w for ν(C_{ar}−C); 1387 s, 1315 s for ν_s-(O−C−O); 1177 m, 1052 m for δ_{ip}(C−H); 923 w for δ_{ring}; 802 m for δ(O−C−O); 775 m for δ_{op} (C−H); 681 m for τ_{ring}; 649 sh for ρ(H_2O); 531 w for π(CO_2); 513 w, 472 w for ν(M−O + M−N). Compound **2**: Anal. Calcd for $C_6H_6FeN_2O_6$: C, 27.91; H, 2.34; N, 10.86; Fe, 21.68. Found: C, 27.81; H, 2.23; N, 10.74; Fe, 21.56. Main IR features (cm^{-1}, KBr pellet): 3262 vs for ν(O−H); 3012 w for ν(C−H); 1667 vs for [ν_{as}(O−C−O) + ν(C═C + C═N)]; 1474 w for ν(C_{ar}−C); 1386 s, 1314 s for ν_s(O−C−O); 1178 m, 1058 m for δ_{ip}(C−H); 937 w for δ $_{ring}$; 816 m for δ(O−C−O); 767 m for δ_{op} (C−H); 697 m for τ_{ring}; 624 m for ρ(H_2O); 544 w for π(CO_2); 518 w, 488 w for ν(M−O + M−N). Compound **3**: Anal. Calcd for $C_6H_6N_2O_6Zn$: C, 26.07; H, 2.27; N, 10.53; Zn, 24.04. Found: C, 26.18; H, 2.30; N, 10.65; Zn, 24.32. Main IR features (cm^{-1}, KBr pellet): 3270 vs for ν(O−H); 3102 w for ν-(C−H); 1667 vs for [ν_{as}(O−C−O) + ν(C═C + C═N)]; 1474 w for ν(C_{ar}−C); 1386 s, 1322 s for ν_s(O−C−O); 1178 m, 1057 m for δ_{ip}(C−H); 940 w for δ_{ring}; 817 m for δ(O−C−O); 777 m for δ_{op} (C−H); 673 m for τ_{ring}; 632 m for ρ(H_2O); 544 w for π(CO_2); 518 w, 496 w for ν(M−O + M−N).

Synthesis of {[Cu(μ-pz25dc)(NH_3)(H_2O)]·H_2O}$_n$ (4) and {[Cu-(μ-pz25dc)(NH_3)$_2$]·2H_2O}$_n$ (5). An aqueous solution (10 mL) of H_2pz25dc·2H_2O (0.612 g, 0.3 mmol) was added dropwise to a stirred solution (water 20 mL) containing $Cu(NO_3)_2$·3H_2O (0.0725 g, 0.3 mmol) and NH_3 (2 mL, 25%). The resulting dark-blue solution was allowed to evaporate at room temperature. A few days later, a mixture of single-crystals of compounds **4** (blue) and **5** (green) was obtained. Compound **4**: Anal. Calcd for C_6H_9-CuN_3O_6: C, 25.49; H, 3.21; N, 14.86; Cu, 22.48. Found: C, 25.32; H, 3.28; N, 14.82; Cu, 22.42. Main IR features (cm^{-1}, KBr pellet): 3388 vs for ν(O−H); 3324 vs, 3261 s for ν(NH_3); 3103 m for ν-(C−H); 1648 vs for [ν_{as}(O−C−O) + ν(C═C + C═N)]; 1473 w for ν(C_{ar}−C); 1385 m, 1319 s for ν_s(O−C−O); 1258 w for δ(H−N−H); 1179 m, 1044 m for δ_{ip}(C−H); 917 w for δ_{ring}; 853 m for δ(O−C−O); 766 w for δ_{op}(C−H); 714 m for ρ(NH_3); 646 m for ρ(H_2O); 575 w for π(CO_2); 514 m, 495 m for ν(M−O + M−N). Compound **5**: Anal. Calcd for $C_6H_{12}CuN_4O_6$: C, 24.04; H, 4.04; N, 18.69; Cu, 21.20. Found: C, 24.30; H, 3.85; N, 18.58; Cu, 21.16. Main IR features (cm^{-1}, KBr pellet): 3436 vs for ν(O−H); 3331 vs, 3241 vs for ν(NH_3); 2928 m, 2851 m for ν(C−H); 1654 vs for [ν_{as}(O−C−O) + ν(C═C + C═N)]; 1480 w for ν(C_{ar}−C); 1375 m, 1319 s for ν_s(O−C−O); 1256 w for δ(H−N−H); 1187 m, 1061 m for δ_{ip}(C−H); 922 w for δ_{ring}; 811 m for δ(O−C−O); 776 m for δ_{op}(C−H); 720 m for ρ(NH_3); 567 w for π(CO_2); 504 w, 498 m for ν(M−O + M−N).

Synthesis of [Mn_2(μ-pz25dc)(phen)$_4$](NO_3)$_2$·10H_2O (6). Compound **6** was prepared in an aqueous solution (30 mL) by the stoichiometric reaction of H_2pz25dc·2H_2O (0.0510 g, 0.25 mmol), $Mn(NO_3)_2$·4H_2O (0.1255 g, 0.5 mmol), and 1,10-phenanthroline (*phen)* (0.1982 g, 1 mmol). The reaction yielded a small amount of a yellow polycrystalline precipitate corresponding to compound **6**. After filtering out the precipitate, the resulting solution was allowed to stand at room temperature. The crystal growth of **6** was observed after 6 days. Yield: 60%. Anal. Calcd for $C_{54}H_{54}$-$Mn_2N_{12}O_{20}$: C, 49.85; H, 4.18; N, 12.92; Mn, 8.44. Found: C, 49.75; H, 4.09; N, 13.05; Mn, 8.33. Main IR features (cm^{-1}, KBr pellet): 3433 vs for ν(O−H); 3050 w for ν(C−H); 1644 s, 1592 sh for [ν_{as}(O−C−O) + ν(C═C + C═N)]; 1518 m for ν(C_{ar}−C); 1426 m, 1304 m for ν_s(O−C−O); 1385 vs for ν_s(NO_3); 1177 w, 1144 w, 1100 w, 1052 w for δ_{ip}(C−H); 848 m for δ_{ring}; 825 m for δ(O−C−O); 774 m for δ_{op}(C−H); 724 m for τ_{ring}; 637 w for ρ-(H_2O); 511 w, 456 w for ν(M−O + M−N).

Synthesis of {(H_2bpe)[Cu(μ-pz23dc)$_2$]·2H_2O}$_n$ (7). Single crystals of **7** were prepared by slow diffusion of an aquo-methanolic solution of H_2pz23dc (0.0504 g, 0.3 mmol) and 1,2-bis(4-pyridyl)-ethylene (*bpe*) (0.0547 g, 3 mmol) into an aqueous solution of Cu-$(NO_3)_2$·3H_2O (0.0725 g, 0.3 mmol). Crystal growth was observed after 5 days. Yield: 65%. Anal. Calcd for $C_{24}H_{20}CuN_6O_{10}$: C, 46.80; H, 3.27; N, 13.64; Cu, 10.32. Found: C, 46.98; H, 3.05; N, 13.85; Cu, 10.25. Main IR features (cm^{-1}, KBr pellet): 3536 vs, 3465 vs for ν(O−H); 3104 w, 3065 w, 3033 w for ν(C−H + N−H); 1642 vs, 1579 m for [ν_{as}(O−C−O) + ν(C═C + C═N)]; 1508 m, 1450 w, 1429 w for ν(C_{ar}−C); 1382 m, 1335 s for ν_s(O−C−O); 1202 w, 1178 w, 1131 m for δ_{ip}(C−H); 1060 w, 887 w for δ_{ring}; 848 m for δ(O−C−O); 738 m for δ_{op}(C−H); 691 m for τ_{ring}; 549 w for π(CO_2); 518 w, 490 w, 447 w for ν(M−O + M−N).

Synthesis of {[Cu_2(μ-pz23dc)$_2$(H_2O)(4apy)$_2$]·2H_2O}$_n$ (8). Single crystals of **8** were synthesized by the slow diffusion of an aquo-methanolic solution of H_2pz23dc (0.0504 g, 0.3 mmol) and 4-aminopyridine (*4apy*) (0.0850 g, 0.9 mmol) into an aqueous solution of $Cu(NO_3)_2$·3H_2O (0.0725 g, 0.3 mmol). Crystal growth was observed after a week. Yield: 75%. Anal. Calcd for $C_{22}H_{22}$-$Cu_2N_8O_{11}$: C, 37.71; H, 3.17; N, 16.00; Cu, 17.98. Found: C, 37.93; H, 3.01; N, 16.17; Cu, 17.88. Main IR features (cm^{-1}, KBr pellet): 3433 vs, 3333 s, 3208 m for ν(O−H + N−H); 3092 w for ν(C−H); 1658 vs, 1625 s, 1575 w for [ν_{as}(O−C−O) + ν(C═C + C═N)]; 1525 m, 1458 w, 1433 w for ν(C_{ar}−C); 1392 s, 1358 m, 1333 m for ν_s(O−C−O); 1216 m, 1133 m for δ_{ip}(C−H); 1067 w, 1025 w for δ_{ring}; 840 w for δ(O−C−O); 750 w for δ_{op}(C−H); 681 m for τ_{ring}; 616 w for ρ(H_2O); 558 w for π(CO_2); 525 w, 483 w, 433 w for ν(M−O + M−N).

Synthesis of {[Cu(μ-pz23dc)(imd)]·3H_2O}$_n$ (9). A methanolic solution of imidazole (*imd*) (0.0408 g, 0.6 mmol) was allowed to diffuse slowly into an aqueous solution of K_2[Cu(pz23dc)$_2$(H_2O)]·6H_2O (0.1800 g, 0.3 mmol). After 2 weeks, the reaction yielded blue single crystals of **9**. Yield: 70%. Anal. Calcd for C_9H_{12}-CuN_4O_7: C, 30.73; H, 3.44; N, 15.93; Cu, 18.06. Found: C, 30.85; H, 3.58; N, 16.11; Cu, 17.85. Main IR features (cm^{-1}, KBr pellet): 3465 vs for ν(O−H + N−H); 3161 m, 3129 m, 3104 m, 3079 m, 2972 w, 2890 w for ν(C−H); 1665 vs, 1608 vs, 1584 s for [ν_{as}-(O−C−O) + ν(C═C + C═N)]; 1452 m for ν(C_{ar}−C); 1378 s, 1345 m for ν_s(O−C−O); 1132 m, 1066 m for δ_{ip}(C−H); 975 w, 950 w for δ_{ring}; 852 w for δ(O−C−O); 753 m for δ_{op}(C−H); 654 w for τ_{ring}; 620 sh for ρ(H_2O); 556 w for π(CO_2); 490 w, 441 w for ν(M−O + M−N).

Physical Measurements. Elemental analyses (C, H, and N) were performed on a LECO CHNS-932 microanalytical analyzer. The metal content was determined by absorption spectrometry. The IR spectra (KBr pellets) were recorded on a FTIR Mattson 1000 spectrometer in the 4000−400 cm^{-1} spectral region. Thermal analyses (thermogravimetry/differential thermogravimetry/differential thermal analysis, TG/DTG/DTA) were performed on a TA Instruments SDT 2960 thermal analyzer in a synthetic air atmosphere (79% N_2/21% O_2) with a heating rate of 5° min^{-1}. Magnetic measurements were performed on polycrystalline samples of the compounds with a Quantum Design SQUID susceptometer covering the temperature range of 5.0−300 K at 0.1 T. The susceptibility data were corrected for the diamagnetism estimated from Pascal's

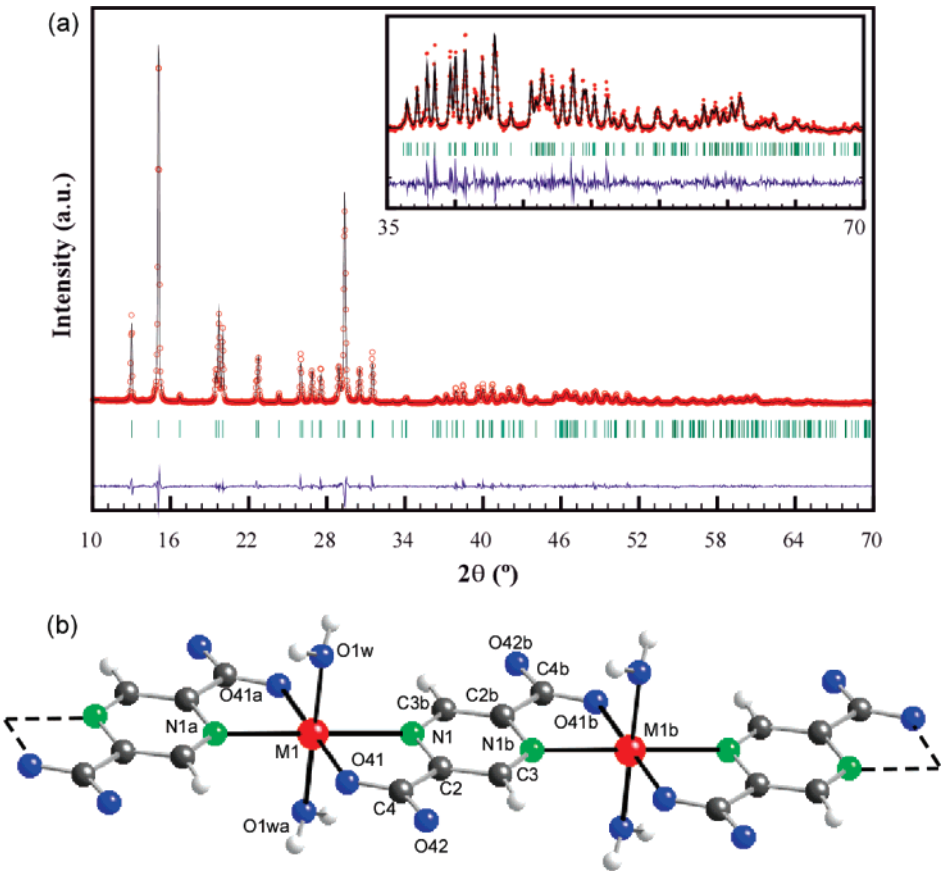

Figure 1. (a) Final Rietveld plot for compound **1** showing observed (dots), calculated (solid line), and difference (lower trace) powder X-ray diffraction patterns. (b) Perspective drawing of a fragment of the one-dimensional chain for compounds **1**−**3**.

tables,[20] the temperature-independent paramagnetism, and the magnetization of the sample holder.

Powder X-ray Diffraction Data Collection and Structure Determination. X-ray powder diffraction data for compounds **1**−**3** were collected on a Phillips X′PERT powder diffractometer with Cu Kα radiation in steps of 0.03° over the 2θ 10−70° range with a fixed-time counting of 40 s at 298 K. The absence of a structural model led us to ab initio resolution of compound **1**. The angular positions of the first 29 peaks of the X-ray powder diffraction pattern were obtained with the WINPLOTR program.[21] An initial triclinic cell was calculated using the DICVOL program.[22] Subsequently, the structureless whole-pattern matching analysis of the diffractogram was carried out for the $P\bar{1}$ space group with the FULLPROF program[23] using the unit cell parameters previously obtained. The integrated intensities were extracted with the FULLPROF program and were used as input in the direct methods program EXPO,[24] which provided a plausible solution. The obtained atomic coordinates were used as the starting model for Rietveld refinement. The atomic coordinates of the hydrogen atoms were geometrically calculated and refined with soft distance constraints.

Table 1. X-ray Powder Crystal Data for Compounds **1**−**3**

	1	**2**	**3**
empirical formula	$C_6H_6MnN_2O_6$	$C_6H_6FeN_2O_6$	$C_6H_6N_2O_6Zn$
fw	257.06	257.97	267.61
cryst syst	triclinic	triclinic	triclinic
space group	$P\bar{1}$	$P1$	$P1$
a (Å)	7.311(1)	7.147(1)	7.034(1)
b (Å)	8.011(1)	7.999(1)	7.900(1)
c (Å)	5.026(1)	5.043(1)	5.082(1)
α (deg)	98.9(1)	99.3(1)	99.5(1)
β (deg)	102.4(1)	102.6(1)	102.6(1)
γ (deg)	127.8(1)	127.4(1)	126.9(1)
V (Å^3)	210.8(3)	206.8(1)	203.8(5)
Z	1	1	1
D_{obs} (g cm^{-3})	1.99(1)	2.05(1)	2.16(1)
D_{calcd} (g cm^{-3})	2.024	2.071	2.179
R_f[a]	3.01	3.14	3.05
R_b[b]	3.12	3.97	3.05
R_p[c]	10.0	12.2	10.4
R_{wp}[d]	13.1	16.0	13.2
χ^2	2.30	1.52	4.88

[a] $R_f = \sum|(I_{obs})^{1/2} - (I_{calcd})^{1/2}|/\sum(I_{obs})^{1/2}$. [b] $R_b = \sum|I_{obs} - I_{calcd}|/\sum I_{obs}$. [c] $R_p = \sum|yi_{obs} - yi_{calcd}|/\sum yi_{obs}$. [d] $R_{wp} = [\sum\omega i|yi_{obs} - yi_{calcd}|^2/\sum\omega i(yi_{obs})^2]^{1/2}$.

The observed and calculated patterns for compound **1** are shown in Figure 1a.

The crystal structure refinements of compounds **2** and **3** were made by means of the FULLPROF program on the basis of the space group, cell parameters, and atomic coordinates found for compound **1**. The crystal parameters and the reliability factors of compounds **1**−**3** are shown in Table 1 (see final Rietveld plots in the Supporting Information).

Single-Crystal X-ray Data Collection and Structure Determination. Data collections on single crystals of compounds **4**−**9**

(20) Earnshaw, A. *Introduction to Magnetochemistry*; Academic Press: London, 1968.
(21) Roisnel, J.; Rodríguez-Carvajal, J. *WINPLOTR*; Laboratoire Léon Brillouin (CEA-CNRS) Centre d'Etudes de Saclay: Gif sur Yvette Cedex, France, 2000.
(22) Boultif, A.; Louder, D. *J. Appl. Crystallogr.* **1991**, *24*, 987−993.
(23) Rodríguez-Carvajal, J. *FULLPROF*, Program Rietveld Pattern Matching Analysis of Powder Patterns; ILL (unpublished), 1997.
(24) Altomare, A.; Burla, M. C.; Camalli, M.; Carrozzini, B.; Cascarano, G.; Giacovazzo, C.; Guagliardi, A.; Moliterni A. G. G.; Polidori, G.; Rizzi R. *J. Appl. Crystallogr*. **1999**, *32*, 339−340.

Table 2. Single-Crystal Data and Structure Refinement Details of Compounds **4**−**9**

	4	**5**	**6**	**7**	**8**	**9**
empirical formula	$C_6H_9CuN_3O_6$	$C_6H_{12}CuN_4O_6$	$C_{54}H_{54}Mn_2N_{12}O_{20}$	$C_{24}H_{20}CuN_6O_{10}$	$C_{22}H_{22}Cu_2N_8O_{11}$	$C_9H_{12}CuN_4O_7$
fw	282.70	299.75	1300.97	616.00	701.56	351.77
cryst syst	monoclinic	triclinic	monoclinic	triclinic	triclinic	monoclinic
space group	$P2_1/c$	$P\bar{1}$	$P2_1/c$	$P\bar{1}$	$P\bar{1}$	$P2_1/c$
a (Å)	6.469(1)	6.285(2)	10.379(1)	6.430(1)	8.319(1)	10.710(3)
b (Å)	12.866(2)	6.857(2)	27.032(2)	8.052(1)	11.904(1)	13.672(3)
c (Å)	12.587(3)	6.950(1)	10.820(1)	11.914(2)	13.646(2)	9.374(2)
α (deg)		71.11(2)		95.26(1)	87.24(1)	
β (deg)	113.96(2)	88.14(2)	107.72(1)	94.99(1)	73.13(1)	93.18(2)
γ (deg)		70.80(2)		98.85(1)	84.15(1)	
V (Å^3)	957.3(3)	266.7(1)	2891.7(4)	603.7(2)	1286.2(3)	1370.5(6)
Z	4	1	2	1	2	4
D_{obs} (g cm^{-3})	1.95(1)	1.86(1)	1.49(1)	1.68(1)	1.80(1)	1.70(1)
D_{calcd} (g cm^{-3})	1.962	1.866	1.494	1.694	1.811	1.705
μ (m^{-1})	2.302	2.073	0.524	0.979	1.732	1.634
R1[a]	0.0315	0.0398	0.0505	0.0431	0.0658	0.0416
wR2[b]	0.0588	0.0980	0.1076	0.1063	0.1188	0.0844

[a] $R1 = \sum(||F_o| - |F_c||)/\sum |F_o|$. [b] $wR2 = [\sum w(||F_o| - |F_c||)^2/\sum w|F_o|^2]^{1/2}$.

were carried out at 293 K with an Xcalibur diffractometer equipped with an area detector and graphite monochromated Mo Kα radiation ($\lambda = 0.710\ 69$ Å). The data reduction was done with the CrysAlis RED program.[25] Information concerning data collection is summarized in Table 2. The structures were solved by direct methods using the SIR97 program.[26] Full-matrix least-squares refinements were performed on F^2 using SHELXL97.[27] All non-hydrogen atoms were refined anisotropically. All calculations were performed using the WinGX crystallographic software package.[28] The final geometrical calculations and the graphical manipulations were carried out with the PARST95[29] and PLATON[30] programs.

Results and Discussion

Description of the Structures. The main structural feature common to compounds **1**−**6** is the presence of octahedrally coordinated M(II) centers sequentially bridged by bis-bidentate *pz25dc* ligands. The bridging ligand forms a five-membered chelate ring with each metal ion by means of an endocyclic nitrogen atom and an oxygen atom from the adjacent carboxylate group. The occurrence of this coordination mode leads to 1-D polymeric chains in compounds **1**−**5** and discrete dimeric entities in compound **6**, where *phen* acts as blocking ligand to avoid further polymerization. In compounds **7**−**9**, the *pz23dc* ligand chelates to a unique copper center, while bridging another one or two metal centers via the remaining carboxylate group. These coordination modes have led to a 1-D linear chain (**7**), 1-D ladder chain (**8**), and 2-D (**9**) covalent frameworks. Selected bond distances, angles, and hydrogen bonding and $\pi-\pi$ interaction data of the described compounds are gathered in the Supporting Information.

[M(μ-pz25dc)(H_2O)$_2$]$_n$ [M = Mn(1), Fe(2), Zn(3)]. Compounds **1**−**3** are isomorphous and crystallize in the triclinic space group $P\bar{1}$. The crystal structures of compounds **1**−**3** consist of one-dimensional polymeric chains running along the [100] direction, in which *trans*-$[M(H_2O)_2]^{2+}$ units are bridged by bis-bidentate *pz25dc* ligands (Figure 1b). In all cases, supramolecular architectures are sustained by means of an intricate network of hydrogen-bond interactions (see the Supporting Information). The intramolecular M−O and M−N distances within the *pz25dc* ligand are similar to those found in the Cambridge Structural Database.[31] Symmetry centers are placed in the metal atom and in the center of the aromatic ring. The metal atom exhibits a distorted octahedral surrounding, in which the basal plane is formed by two carboxylate O atoms from two *pz25dc* ligands [M1−O41 = 2.16(1), 2.12(2), and 2.04(2) Å for **1**, **2**, and **3**] and two water molecule O atoms [M1−O1w = 2.14(1), 2.14(2), and 2.01(2) Å]. This plane is almost perpendicular to the mean plane of the pyrazine ring (ca. 86.3°). The axial positions are filled by two nitrogen atoms with slightly greater bond distances [M1−N1 = 2.28(2), 2.309(3), and 2.15(3) Å]. The M···M distance through the μ-pyrazine bridge ranges from 7.03 to 7.31 Å (the value of the *a* crystallographic axis). The M(II) atoms show a small displacement from the mean plane of the bridging ligand (ca. 0.08 Å). In fact, the *pz25dc* ligand is essentially planar with a dihedral angle between the carboxylate group and the aromatic ring of 7.1(3), 2.2(4), and 7.2(3)° in compounds **1**, **2**, and **3**, respectively. The bridging ligand forms one five-membered chelate ring with each metal [bite angles: 75.1(6), 77.7(7), and 80.5(7)°, respectively].

In the crystal building, each chain interacts with four adjacent chains (Figure 2) by means of hydrogen bonding interactions involving the coordination water molecules and oxygen atoms of the carboxylate groups. For comparative purposes, the crystal structure of these compounds can be alternatively described as the piling up of layers of polymeric chains linked by the hydrogen bond established by the noncoordinated oxygen atom of the carboxylate group and

(25) *CrysAlis RED*, version 1.170; Oxford Diffraction: Wroclaw, Poland, 2003.
(26) Altomare, A.; Burla, M. C.; Camalli, M.; Cascarano, G. L.; Giacovazzo, C.; Guagliardi, A.; Moliterni, A. G. G.; Spagna, R. *J. Appl. Crystallogr.* **1999**, *32*, 115−119.
(27) Sheldrick, G. M. *SHELXS97* and *SHELXL97*; University of Göttingen: Göttingen, Germany, 1997.
(28) Farrugia, L. J. *WINGX. A Windows Program for Crystal Structure Analysis*; University of Glasgow: Glasgow, Scotland, 1998.
(29) Nardelli, M. *J. Appl. Crystallogr.* **1995**, *28*, 659.
(30) Spek, A. L. *PLATON, a Multipurpose Crystallographic Tool*; Utrecht University: Utrecht, Holland, 1998.
(31) Allen, F. H. *Acta Crystallogr., Sect. B* **2002**, *58*, 380−388.

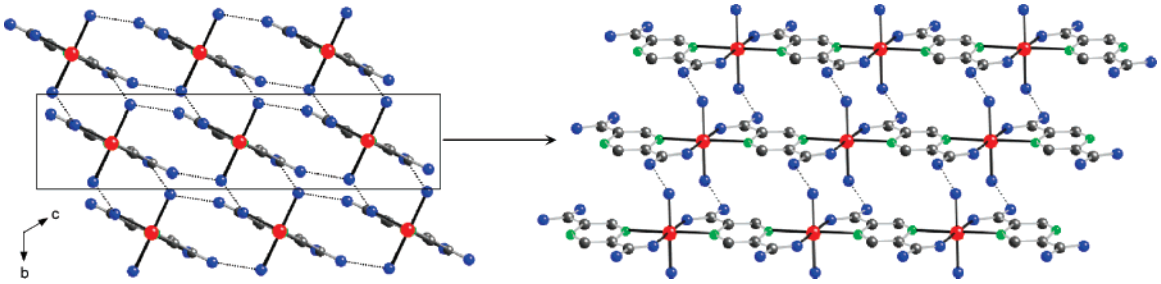

Figure 2. View of the crystal packing (left) along the [100] direction of compounds **1**−**3**, showing the two-dimensional arrangement of polymeric chains (right). Dotted lines represent the hydrogen-bonding scheme. Hydrogen atoms were omitted for clarity.

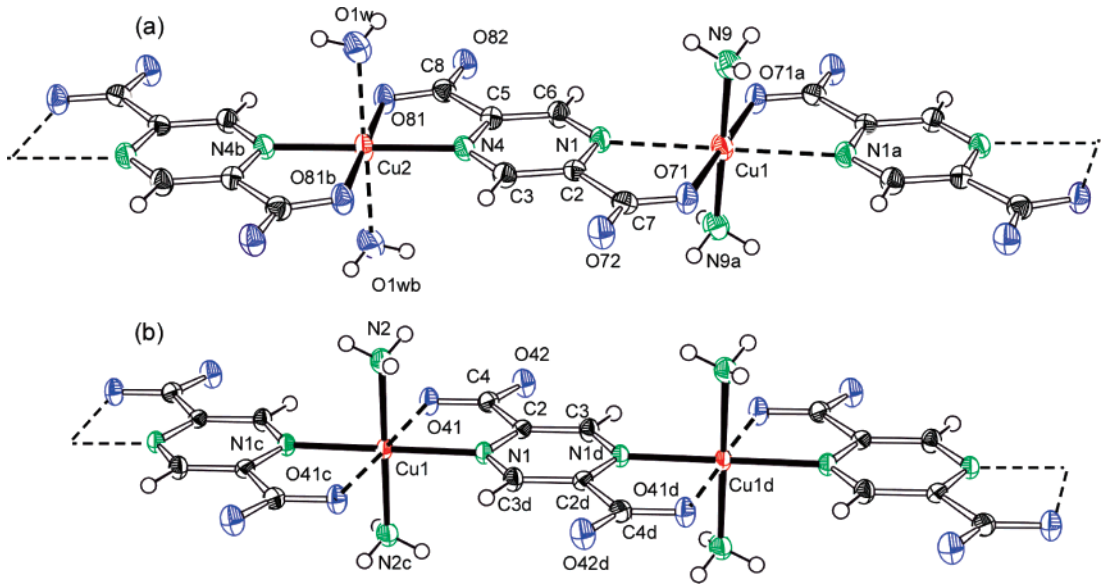

Figure 3. Perspective drawing of a fragment of the one-dimensional chain for compounds **4** (a) and **5** (b).

the coordination water molecule (O1w···O42, ca. 2.71 Å; O1w−H11···O42, ca. 150°). These layers are held together by means of an additional hydrogen bond established by the coordinated oxygen atom of the carboxylate group and the coordination water molecule. As we will see later on, this is a common feature in all 1-D complexes based on the *pz25dc* bridging ligand reported herein.

{[Cu(*μ*-pz25dc)(NH$_3$)(H$_2$O)]·H$_2$O}$_n$ (4) and {[Cu(*μ*-pz25dc)(NH$_3$)$_2$]·2H$_2$O}$_n$ (5). Compounds **4** and **5** crystallize in the $P2_1/c$ and $P\bar{1}$ space groups, respectively. The molecular structures of these compounds show some similarities with those described previously. Both consist of one-dimensional polymeric chains in which metal centers are linked by bis-bidentate *pz25dc* ligands (Figure 3). However, the typical Cu(II) tetragonally elongated octahedral coordination environments present some differences. The crystal structure of compound **4** presents one *pz25dc* ligand and two crystallographically independent copper atoms with symmetry centers sited on the metals. The apical positions along the chain are occupied by ammonia and water molecules in an alternated way. In compound **5**, there is only one *pz25dc* ligand and one copper atom crystallographically distinguishable, and the symmetry centers are placed on the metal atoms and in the center of the aromatic ring. The ammonia molecule is the unique terminal ligand coordinated to the metal ion.

In compound **4**, the Cu1 atom forms two five-membered chelate rings with two *pz25dc* ligands related by the symmetry center located in the metal [bite angle = 73.99(8)°]. The coordination sphere is completed by two ammonia molecules. The equatorial plane involves the nitrogen atoms of two ammonia molecules and two oxygen atoms from carboxylate groups of two *pz25dc* ligands [Cu1−N9 = 1.993(3) Å, Cu1−O71 = 1.994(2) Å]. This plane is nearly perpendicular to the mean plane of the pyrazine ring [dihedral angle = 86.4(1)°]. The occurrence of the Jahn−Teller effect leads to two substantially longer bond distances formed by the endocyclic nitrogen atoms of the *pz25dc* ligand [Cu1−N1 = 2.469(2) Å]. The Cu1 atom lies nearly coplanar to the mean plane of the pyrazine with a deviation of 0.0156(2) Å. In the case of the Cu2 atom, the ammonia molecules are replaced by two water molecules, which form the two largest bond distances [Cu2−O1w = 2.373(2) Å]. The Cu2 atom forms two five-membered chelate rings with a bite angle of 83.08(8)°. The equatorial plane is formed by two nitrogen atoms and two oxygen atoms from the adjacent carboxylate group of two *pz25dc* ligands [Cu2−N4 = 2.019(2) Å, Cu2−O81 = 1.947(2) Å]. For that reason, the equatorial plane is almost coplanar to the mean plane of the bridging ligand [dihedral angle = 1.70(8)°]. The deviation of Cu2 from the mean plane of the pyrazine ring is 0.0407(2) Å. The *pz25dc* ligand remains essentially planar, and the dihedral angles between the aromatic ring and the carboxylate groups are 2.3(2) and 0.3(2)°.

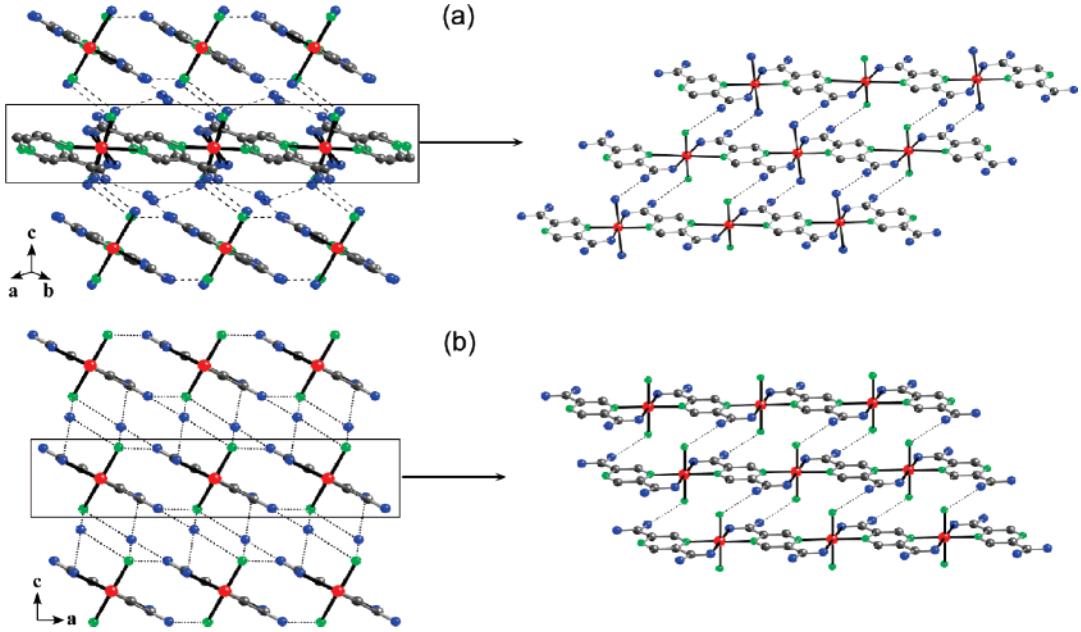

Figure 4. View of the crystal packing (left) of compounds **4** (a) and **5** (b), showing the two-dimensional arrangement of polymeric chains (right). Dotted lines represent the hydrogen-bonding scheme. Hydrogen atoms were omitted for clarity.

Compound **5** is comprised of *trans*-$[Cu(NH_3)_2]^{2+}$ units sequentially joined by bis-bidentate *pz25dc* ligands and two crystallographically independent solvated water molecules. The CuO_2N_4 chromophore can be described as the usual elongated tetragonal octahedron with four short distances [Cu1−N1 = 2.053(2) Å, Cu1−N2 = 2.011(3) Å] and two long ones [Cu1−O41 = 2.325(2) Å]. The equatorial plane is nearly perpendicular to the mean plane of the bridging ligand [dihedral angle = 87.1(2)°]. The deviation of the Cu1 atom from the least-squares plane of the pyrazine ring is negligible [0.0010(4) Å], and the dihedral angle between the pyrazine ring and the carboxylate group is 2.3(2)°.

As previously mentioned, each copper atom forms two five-membered chelate rings with two *pz25dc* ligands in the trans position. Because of the Jahn−Teller effect, the bite angle value can vary substantially depending on the direction of the elongation. In the case of the Cu1 atom of compounds **4** and **5**, the elongation takes place in the direction of one of the donor atoms of the bridging ligand, which leads to bite angles of 73.99(8) and 76.23(7)°, respectively. On the contrary, the elongation in the Cu2 atom of compound **4** occurs in the direction of the terminal ligand, leading to a greater bite angle [83.08(8)°]. In addition, this effect can be observed in the M···M distance through the pyrazine bridge. Compound **4** shows the greatest M···M distance (Cu1···Cu2 = 7.200 Å) because the elongation is located in one of the nitrogen atoms of the bridging ligand. However, in compound **5**, the nitrogen atom of the bridging ligand is not involved in the elongation, which results in a shorter M···M distance (Cu1···Cu1 = 6.857 Å).

In all of the complexes cited above, the location of the aromatic ring within the chain does not allow the establishment of $\pi-\pi$ interactions, so the supramolecular structure is built up by the occurrence of hydrogen-bonding interactions (see the Supporting Information). The likeness of the one-dimensional polymeric chains leads to some similarities in the scheme of noncovalent interactions. The molecular chains are linked together by means of one hydrogen bond involving the coordination water or ammonia molecules and the noncoordinated oxygen atoms of the *pz25dc* ligand from an adjacent chain (hydrogen bonding contacts ca. 2.92 Å and 164° for D···A and D−H···A, respectively), giving rise to a similar two-dimensional array of chains (Figure 4) which pile up one above the other. This two-dimensional arrangement of the chains can be observed in compounds **1**−**3** as well (Figure 2). In complexes **4** and **5,** crystallization water molecules are inserted into the interlayer space linking chains from adjacent layers by means of a hydrogen-bonding network. The alternation of water and ammonia molecules along the polymeric chain in compound **4** leads to a complex scheme of noncovalent interactions between the layers of chains and crystallization water molecules. Herein, an array of layers regularly alternated along the *c* axis can be observed. Chains within the layer located in the $z = 0$ level extend along the [1−10] direction, while the chains of the upper layer located at $z = {}^1/_2$ extend along the [110] direction. Thereby, the crossing between chains of adjacent layers leads to an angle of 53.4° (see the Supporting Information). The chains of different layers are hydrogen-bonded by means of the coordinated water and ammonia molecules each time they cross (N9···O1w = 3.101 Å, N9−H91···O1w = 174°). Each crystallization water molecule is tetrahedrally attached to four surrounding polymeric chains by means of hydrogen-bonding interactions, two from an upper layer (N9···O2w = 3.146 Å, N9−H93···O2w = 167°; O2w···O82 = 2.805 Å, O2w−H22···O82 = 158°) and two from a lower layer (O1w···O2w = 2.758 Å, O1w−H11···O2w = 174°; O2w···O72 = 3.011 Å, O2w−H21···O72 = 165°).

$[Mn_2(\mu$-pz25dc)(phen)$_4](NO_3)_2\cdot 10H_2O$ (6). Compound **6** crystallizes in the $P2_1/c$ space group, and it is isomorphous to the analogous Cu(II) complex recently reported by our research group.[9] The structure consists of crystallization water

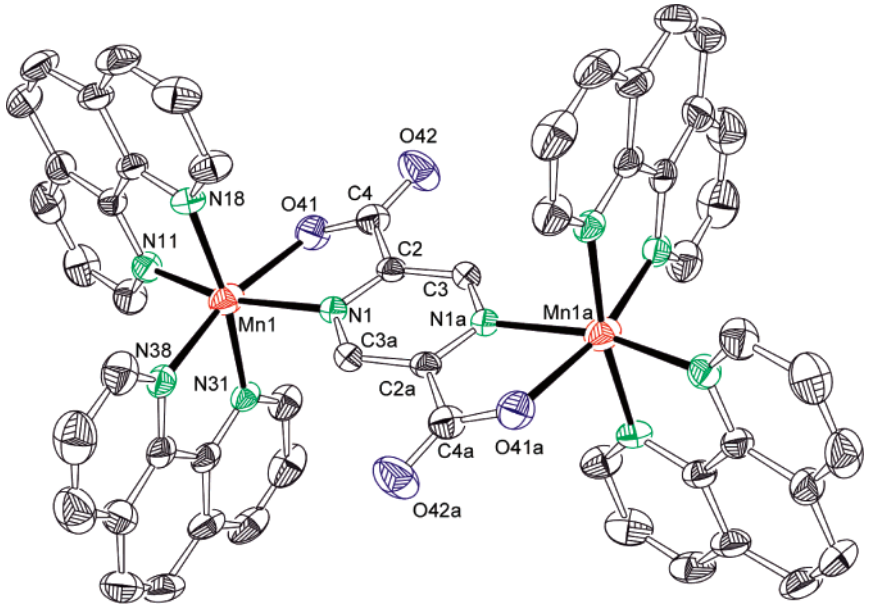

Figure 5. ORTEP view of the dimeric entity in compound **6**.

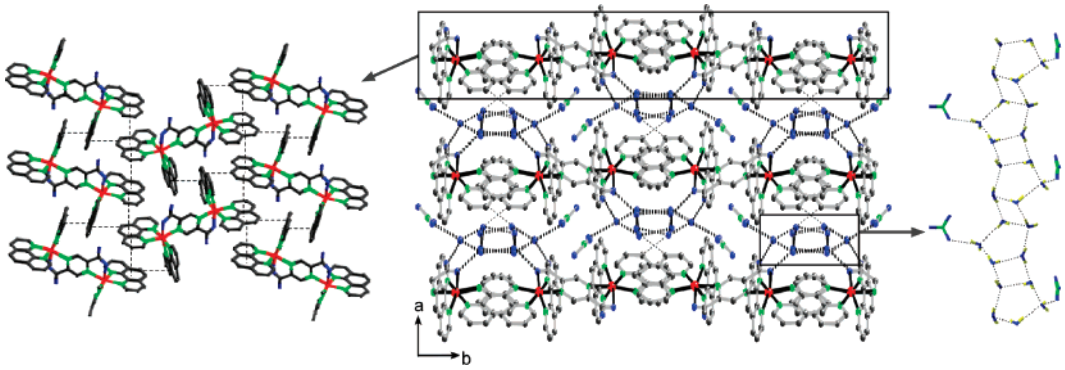

Figure 6. Crystal structure of compound **6** viewed along the [001] direction showing $\pi-\pi$ interactions (dashed lines) within the cationic layers and hydrogen-bonded (dotted lines) tapes of water molecules.

molecules, nitrate counterions, and centrosymmetric $[Mn_2(\mu\text{-pz25dc})(phen)_4]^{2+}$ binuclear units (Figure 5) in which a bis-bidentate *pz25dc* ligand bridges two manganese atoms with a M···M distance of 7.328 Å. The distorted octahedral environment around each manganese atom is completed by four nitrogen atoms of two *phen* ligands (*phen1* and *phen2*). The *pz25dc* ligand coordination bond distances are 2.149(2) and 2.302(3) Å for the oxygen and nitrogen atoms, respectively, while the Mn−N distances implying the phenanthroline ligands are within the 2.221−2.252 Å range. The deviation of the metal atom from the pyrazine ring is quite significant [0.314(1) Å] probably because of the steric hindrance of the terminal ligands. The *pz25dc*, *phen1*, and *phen2* bite angles are 74.4(1), 75.0(1), and 74.5(1)°, respectively.

In the crystal building (Figure 6), the cationic complexes hold together by means of face-to-face and edge-to-face $\pi-\pi$ interactions among the aromatic *phen* ligands to form corrugated layers parallel to the *bc* plane. The water molecules are inserted in the interlayer space and are linked themselves by Ow−H···Ow hydrogen bonds to form *zigzag* tapes comprised of an alternated sequence of fused water pentamers and tetramers [T5(2)4(2)] running along the [001] direction (hydrogen-bonding contacts ca. 2.85 Å and 165° for Ow···Ow and Ow−H···Ow, respectively) in which five crystallographically independent water molecules are repeated by a glide plane to afford this kind of tape structure. Among the different tapelike patterns of water clusters found in hydrated compounds,[32] the water tape of compound **6** has a very low frequency of occurrence, and the predominant ones consist of linked five-membered rings [T5(2)] or alternate four- and six-membered rings [T6(2)4(2)] sharing one edge. In compound **6**, the water molecules shared between the pentamers and tetramers establish three hydrogen bonds with other water molecules within the tape, while the remaining one establishes only two (Figure 7). The remaining positions of the tetrahedral hydrogen-bonding environment are completed for O1w, O2w, and O4w with atoms of the complex cation or the nitrate anion. O3w and O5w remain three-coordinated. The volume corresponding to these water channels is ca. 19.9% of the unit cell.[30] The nitrate anions are hydrogen-bonded to the edges of the water pentagonal ring. There is not any significant interaction between adjacent strips. Thereby, the water tapes act as bridges between the

(32) Infantes, L.; Motherwell, S. *CrystEngComm* **2002**, *4*, 454−461.

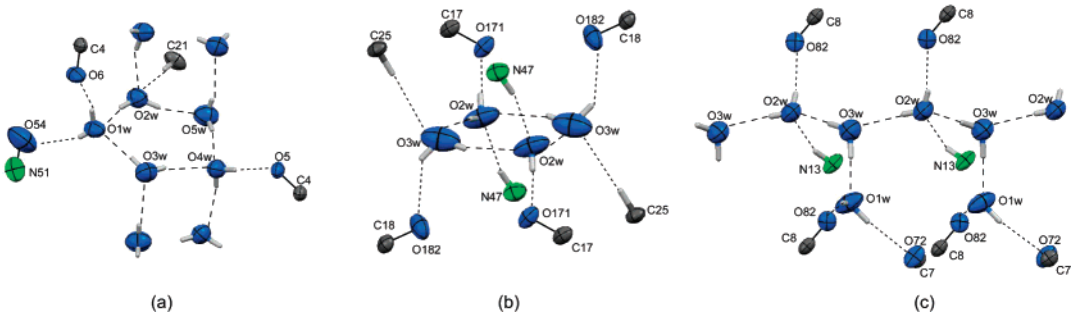

Figure 7. Water clusters in compounds **6** (a), **8** (b), and **9** (c) showing their immediate environment.

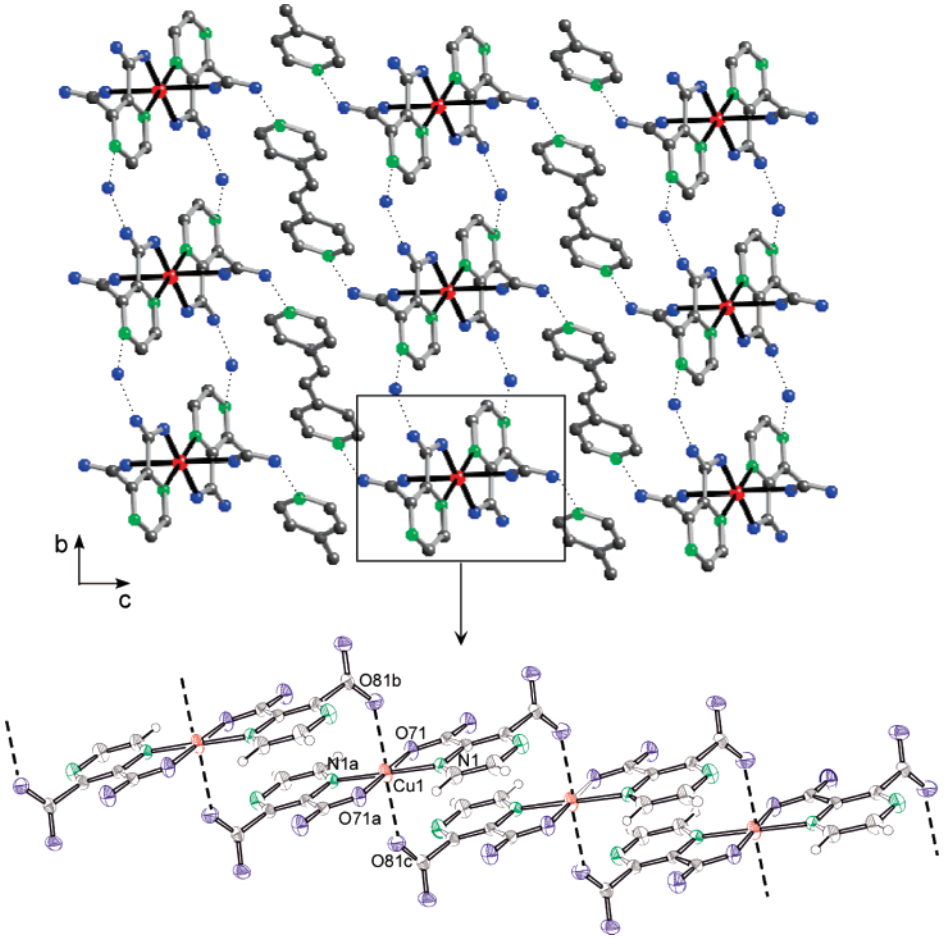

Figure 8. View of the crystal packing (top) along the [100] direction of compound **7**, showing a fragment of the one-dimensional chain (bottom). Dotted lines represent the hydrogen-bonding scheme.

cationic layers by means of a highly complex network of noncovalent interactions. Compound **6** shows a different crystal packing than those described in a recent study[33] of the most common packings of complexes based on *phen* ligands and bears a very close resemblance to the compound $\{[Cu(ox)(phen)_2]\cdot 5H_2O\}$.[34] Both compounds show a similar $\pi-\pi$ interaction scheme within the corrugated complex layers. Because of this conformation, there is a likeness between the hydrophilic holes in the interlayer space, which leads to a similar arrangement of the solvated water molecules.

(33) Russel, V.; Scudder, M.; Dance, I. *J. Chem. Soc., Dalton Trans.* **2001**, 789−799.
(34) Castillo, O.; Luque, A.; Román, P. *J. Mol. Struct.* **2001**, 181−188.

$\{(H_2bpe)[Cu(\mu\text{-pz23dc})_2]\cdot 2H_2O\}_n$ (7). Compound **7** crystallizes in the $P\bar{1}$ space group, and its crystal structure is comprised of $(H_2bpe)^{2+}$ cations, $\{[Cu(pz23dc)_2]^{2-}\}_n$ anionic chains (Figure 8), and crystallization water molecules. The polymeric chain can be described as the piling up of $[Cu(pz23dc)_2]^{2-}$ entities linked among them by the oxygen atom (O81) of a carboxylate group belonging to a neighboring anionic entity. Each copper atom is located at the center of an elongated octahedron as result of a pronounced Jahn−Teller effect. The basal plane consists of two nitrogen atoms [Cu1−N1 = 1.978(2) Å] and two oxygen atoms [Cu1−O71 = 1.954(1) Å] belonging to two *pz23dc* ligands related by the inversion center sited at the copper atom. The two apical positions are occupied by two oxygens [Cu1−O81 = 2.469-

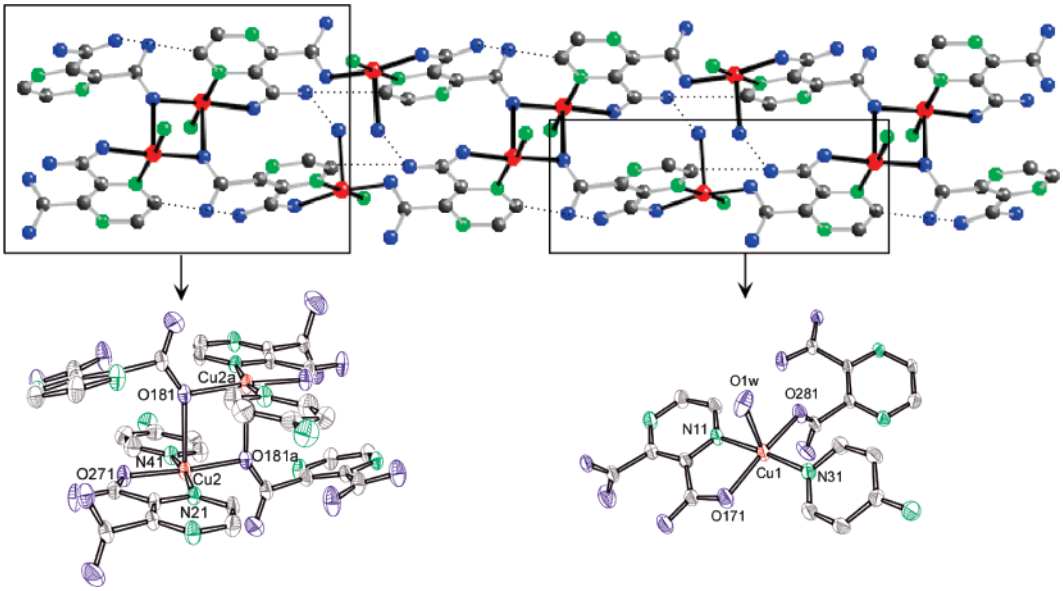

Figure 9. Perspective view of a polymeric ladder chain in compound **8** showing ORTEP drawings of the Cu atom coordination environment. Dotted lines represent intramolecular hydrogen bonding. The noncoordinated atoms of the *4apy* molecule have been omitted for clarity.

(2) Å] of two symmetry-related *pz23dc* ligands belonging to two neighboring $[Cu(pz23dc)_2]^{2-}$ entities. The shortest Cu···Cu distance within the polymeric chain agrees with the value of the *a* crystallographic axis [6.430(1) Å]. The displacement of the Cu(II) atom from the mean plane of the pyrazine ring is 0.1256(1) Å. The *pz23dc* ligand chelates the Cu(II) atom via the heterocyclic N atom and the O atom of the adjacent carboxylate group [bite angle = 83.12(6)°], while the remaining carboxylate group is linked to another Cu(II) atom of a neighboring unit in a monodentate fashion via one of its oxygens. The carboxylate group involved in the chelation is almost coplanar to the pyrazine ring [dihedral angle of 4.25(2)°], while the other is almost perpendicular [dihedral angle of 81.39(1)°]. This chain conformation has been previously observed in other copper(II) complexes of hydrogenpyrazine-2,3-dicarboxylate.[35]

The supramolecular architecture of compound **7** is sustained by means of an intricate network of noncovalent interactions between the cationic entities, the anionic chains, and the crystallization water molecules. The anionic $\{[Cu(pz23dc)_2]^{2-}\}_n$ chains run along the *a* axis and form a two-dimensional array of chains parallel to the *ab* crystallographic plane. Crystallization water molecules connect adjacent polymeric chains by the establishment of hydrogen-bonding interactions (O1w−H1w···O72 and O1w−H2w···N4). The $(H_2bpe)^{2+}$ cations are inserted between two parallel arrays of chains giving rise to a pillared structure which acts as a hydrogen-bond donor linking upper and lower arrays of chains (N11−H11···O82).

$\{[Cu_2(\mu\text{-pz23dc})_2(H_2O)(4apy)_2]\cdot 2H_2O\}_n$ (8) and $\{[Cu(\mu\text{-pz23dc})(imd)]\cdot 3H_2O\}_n$ (9). Compounds **8** and **9** crystallize in the $P\bar{1}$ and $P2_1/c$ space groups, respectively. Although in compound **8** there are two crystallographically independent copper(II) atoms and *pz23dc* ligands versus only one independent metal center and *pz23dc* ligand in compound **9**, their crystal structures present some similarities, which allows a common description. In both compounds, the copper atoms present an elongated square-pyramidal coordination (4 + 1) (Figures 9 and 10). The basal plane, which involves the shortest bonds, is formed by a chelating *pz23dc* ligand (NX1, 1.993−2019 Å and OX71, 1.937−1.977 Å; bite angle ca. 81.9°), the endocyclic N atom of the terminal ligand, *4apy* in **8** and *imd* in **9** (NX1, 1.947−1.985 Å), and the oxygen atom of the nonchelating carboxylate group of another *pz23dc* ligand (OX81, 1.963−1.980 Å). The longer apical bond is established with the oxygen atom of a water molecule [2.300(3) Å in **8**] or of a *pz23dc* ligand [2.498(3) Å in **8** and 2.467(2) Å in **9**]. As described for complex **7**, the carboxylate groups involved in the chelation are almost coplanar with the pyrazine ring (dihedral angle: 1.47−7.99°), while the other one is almost perpendicular (dihedral angle: 78.33−89.04°).

Taking into account only the basal bonds, both compounds are built up of 1-D polymeric chains in which the *pz23dc* ligands bridge two metal centers in the same manner: each *pz23dc* ligand forms a five-membered chelate ring with the first metal center involving one N and one O atom of the adjacent carboxylate group and binds to a second copper(II) atom in a monodentate mode through an O atom of the remaining carboxylate group. The main structural difference between both compounds involves the apical bonds. In compound **8**, the apical position of the coordination sphere in Cu1 is occupied by a water molecule, which precludes further polymerization, and in Cu2, the apical bond is established with the previously equatorially bonded O atom of the nonchelating carboxylate group of the *pz23dc* ligand belonging to the adjacent equatorially bonded chain. This extra polymerization involves two symmetry-center-related Cu2 atoms and forms bis(μ-oxo)-bridged binuclear subunits. This coordination-bond pattern leads to a ladderlike chain

(35) Patrick, B. O.; Stevens, C. L.; Storr, A.; Thompson, R. C. *Polyhedron* **2003**, *22*, 3025−3035.

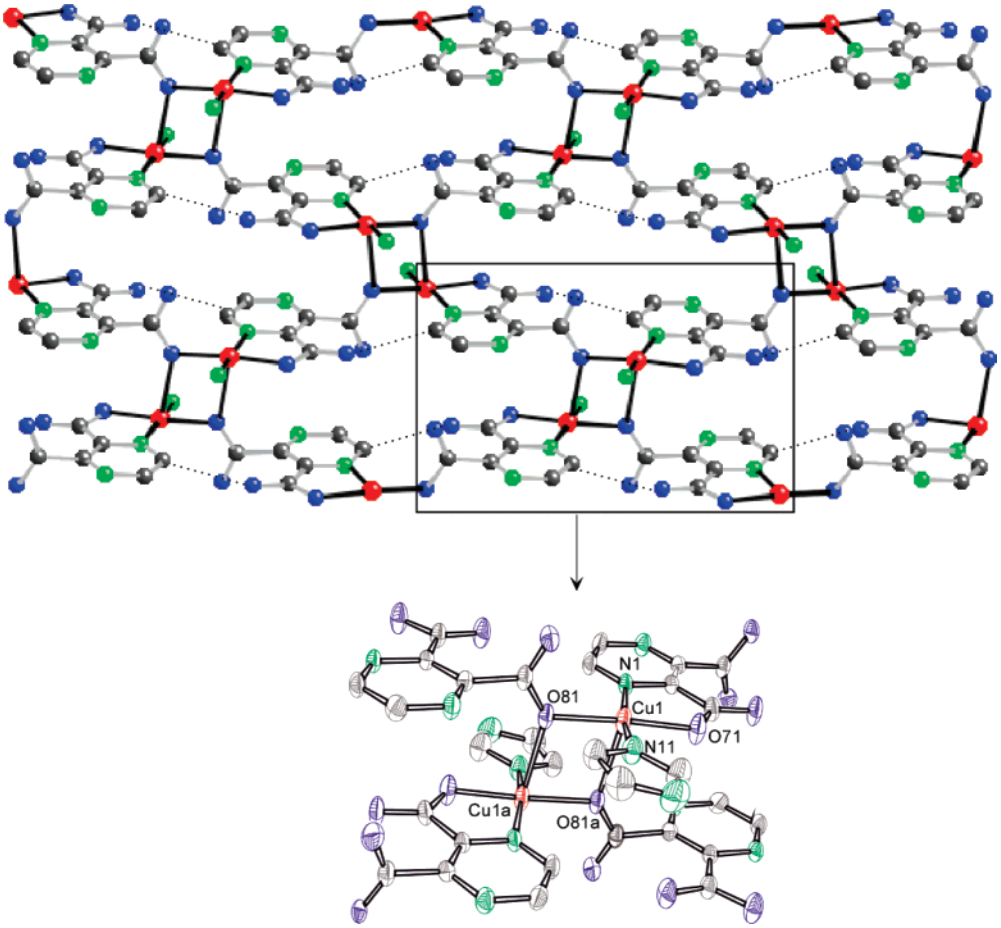

Figure 10. Perspective view of a polymeric layer in compound **9** showing an ORTEP drawing of the Cu atom coordination environment. Dotted lines represent intramolecular hydrogen bonding. The noncoordinated atoms of the *Imd* molecule have been omitted for clarity.

structure (Figure 9). In compound **9**, the metal centers complete their apical position through the equatorially bonded O atom of the nonchelating carboxylate group of the *pz23dc* ligand belonging to the adjacent chains, leading to a 2-D overall structure (Figure 10).

As can be observed in Figures 9 and 10, both complexes show intramolecular hydrogen-bonding interactions involving the coordinated water molecule, the carboxylate free oxygen, and the aromatic H atom of the pyrazine ring in compound **8** (O1w−H···O272, C16−H16···O272, and C26−H26···O172) and the carboxylate free oxygen and aromatic H atom of the pyrazine ring in compound **9** (C6−H6···O72).

Finally, the cohesiveness of the three-dimensional building of compounds **8** and **9** is maintained by means of an extensive hydrogen-bonding network. The polymeric ladder chains of compound **8** run along the *c* crystallographic axis, and each chain is surrounded by four other chains (Figure 11). The crystal packing of the chains generates channels along the *a* axis, which are occupied by crystallization water molecules. These crystallization water molecules are assembled to form isolated hydrogen-bonded water tetramers. In compound **9**, the 2-D [Cu(μ-pz23dc)(imd)] sheets pile up one above the other parallel to the *bc* crystallographic plane (Figure 12). This packing generates interlayer spaces (ca. 22.4%) in which water molecules are inserted and form hydrogen-bonded 1-D chains running along the *c* axis. These water chains act as a bridge between upper and lower polymeric layers providing the cohesiveness to the supramolecular structure. The water array found in compound **8** consists of four-membered water rings [R4] with C_i symmetry (Figure 7), which is in good concordance with the predominant pattern found for discrete clusters.[32] Nonetheless, it is unusual[36] for MOFs that, on one hand, the water molecules are linked together via hydrogen bonds in the same way as tetramers in the gas phase[37] and, on the other hand, the tetramer itself is embedded in a tetrahedral interaction network such as that known from ice structures.[38] Within the tetrameric cluster, each water molecule acts as one hydrogen-bond donor and one hydrogen-bond acceptor, and it completes the tetracoordination interacting with the donor/acceptor groups of the MOF. Hydrogen-bonding contacts within our tetramer (ca. Ow···Ow, 2.78 Å; Ow−H···Ow, 173°; H−Ow−H, 110°) are comparable to that found in ice I_h (2.75 Å, 180°, and 109.5°)[39] and shorter than those corresponding to other tetramers[36,40] found in the solid state

(36) Zuhayra, M.; Kampen W. U.; Henze, E.; Soti, Z.; Zsolnai, L.; Huttner, G.; Oberdofer F. *J. Am. Chem. Soc.* **2006**, in press.
(37) Liu, K.; Cruzan, J. D.; Saykally, R. J. *Science* **1996**, *271*, 929−933.
(38) (a) Peterson, S. W.; Levy, H. A. *Acta Crystallogr.* **1957**, *10*, 70−76. (b) Fletscher, N. H. *The Chemical Physics of Ice*; Cambridge University Press: Cambridge, U. K., 1970.
(39) Ludwing, R. *Angew. Chem., Int. Ed.* **2001**, *40*, 1808−1827.

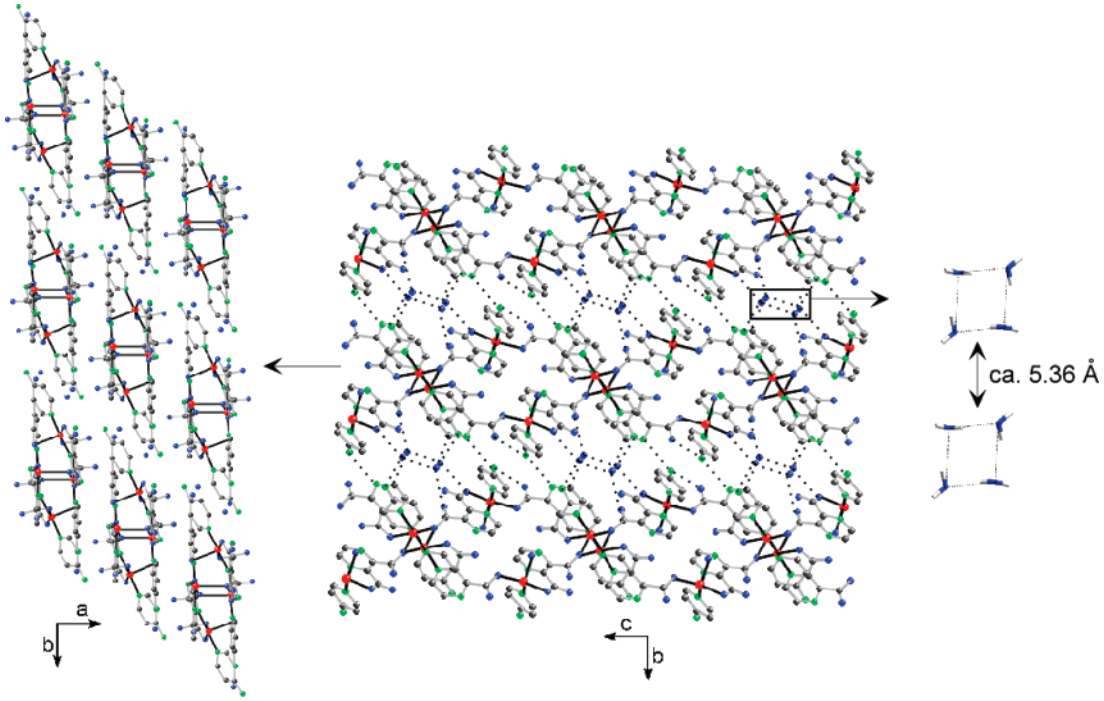

Figure 11. Crystal structure of compound **8**: ladder chains running along the *c* axis (left), intermolecular hydrogen bonding (center), and water tetramers (right).

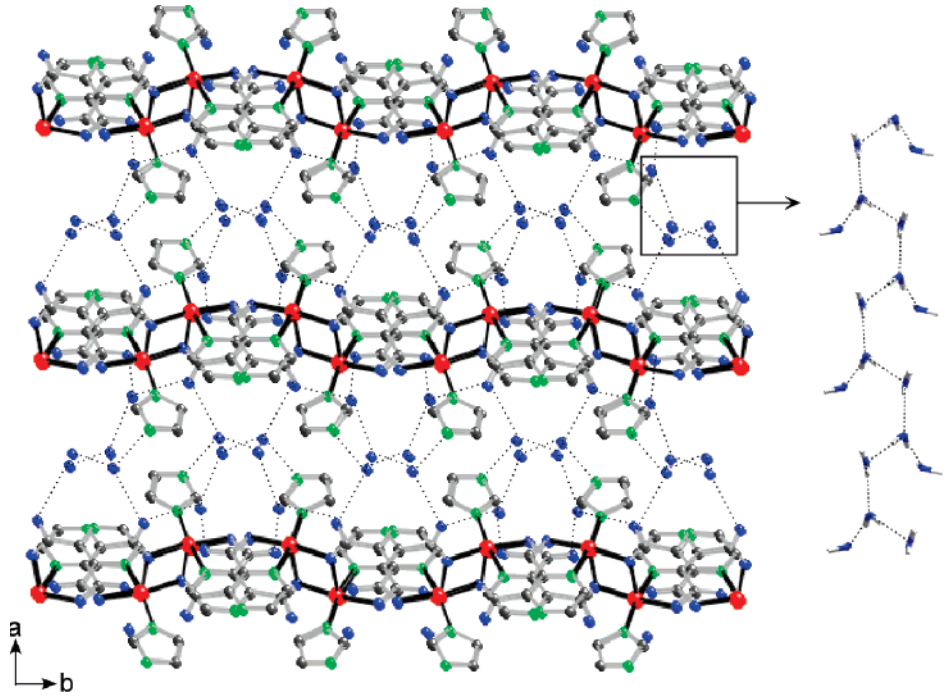

Figure 12. Crystal structure of compound **9** viewed along the *c* axis showing hydrogen-bonded (dotted lines) chains of water molecules.

(ca. 2.82 Å). In the case of water chains, the greatest frequency of occurrence is that with repeating units of four molecules [C4], but although the pattern of the water chain observed in compound **9** (Figure 7) can be related to this, it presents an additional water molecule attached to the chain through a single hydrogen bond. The crystallographically independent water molecules (O1w, O2w, and O3w) are repeated by a glide plane to give the water chain pattern found in compound **9** (ca. Ow···Ow, 2.77 Å and Ow-H···Ow, 170°). As far as we know, this pattern of water array has not been previously reported. One of the water molecules (O2w) shows a tetrahedral coordination, while the other ones (O1w and O3w) establish three hydrogen-bonding interactions. O2w is hydrogen-bonded to two symmetrically related O3w water molecules and completes its tetracoordination

(40) (a) Sun, J. Q.; Zang, J.; Ju, Z. F.; Yang, G. Y. *Aust. J. Chem.* **2005**, *58*, 572−577. (b) Long, L. S.; Wu, Y. R.; Huang, R. B.; Zheng, L. S. *Inorg. Chem.* **2004**, *43*, 3798−3800. (c) Tao, J.; Ma, Z. J.; Huang, R. B.; Zheng, L. S. *Inorg. Chem.* **2006**, in press.

with the donor/acceptor groups of an upper 2-D [Cu(μ-pz23dc)(imd)] layer, while O1w is hydrogen-bonded to one O3w and two acceptor groups of a lower layer. O3w only interacts with water molecules within the cluster, two symmetry related O2w's, and one O1w.

To conclude the structural section, we would like to emphasize some remarkable differences between the coordination features of these bridging ligands and the structures they generate. The absence of a steric hindrance between the carboxylate in *pz25dc* favors the bis-bidentate coordination mode, which is the key feature that allows the straightforward design and synthesis of one-dimensional polymeric complexes or discrete polynuclear entities when blocking ligands are employed. However, the use of hydrothermal synthesis conditions can increase the coordination denticity of *pz25dc*, leading to metal-organic networks of higher dimensionality.[8] The steric hindrance between the carboxylate groups in *pz23dc* causes the twisting of one or both carboxylate groups, enabling the multiple coordination modes that this ligand presents (see the Supporting Information). Despite this structural feature is a drawback for the bis-chelated coordination fashion (D-1) and therefore constructing analogous systems to the *pz25dc* complexes, it contributes to the synthesis of higher-dimensionality networks. The selection of the metal ion and additional terminal or bridging ligands exerts a great influence on the coordination mode of the *pz23dc* bridging ligand and, therefore, on the dimensionality of the covalent network.

On the other hand, the presence of crystallization water molecules within the structure can play an important role in the stabilization of supramolecular architectures because the numbers of donors and acceptors can differ significantly from those of the anhydrous compounds. Therefore, the hydrogen-bonding interactions of the donor/acceptor groups of the organic molecules with the water molecules are crucial in the overall covalent structure as occurs in compounds **8** (1-D complex) and **9** (2-D complex), but in the same way, the arrangement of water molecules varies significantly, giving rise to different cluster patterns. So, often, it might be difficult to decide if the metal-organic framework directs the pattern of the water cluster or if water templates the overall crystal structure,[41] but it can be regarded as the cocrystallization of a complex entity (Cu-*pz23dc*-B, B = *4apy*, *imd*) and water.

The analysis of the crystal structures of compounds **6**, **8**, and **9** clearly shows that water clusters are located in unobstructed channels, which could allow a straightforward release of water molecules and even a reversible transport of them. To analyze this possible reversibility of the dehydration process, thermoanalytical gravimetry and thermodiffractometry measurements (Figure 13) have been performed for the above-cited compounds. In all of them, thermal analysis reveals that the release of water molecules starts at almost room temperature (ca. 35 °C), and it is completely ended when the temperature has reached ca. 100 °C. In all cases, at room-temperature, X-ray powder diffraction (XRPD) patterns match the simulated patterns generated from the crystal structures. In compound **6**, the loss of water molecules at 60 °C agrees with the structural change revealed by the XRPD pattern at 60 °C. The XRPD pattern of the anhydrous phase remains invariable up to 150 °C. The thermodiffractometry measurements in compound **8** show that the release of water tetramers leads to minor changes in the XRPD patterns within the range of 20−70 °C. Nonetheless, a small displacement of [010] reflection to higher values of 2θ is observed. This displacement can be related to the compression of the *b* parameter ($T = 70$ °C, $\Delta 2\theta = 0.211°$, $\Delta d = 0.329$ Å) because of the approximation of layers of chains parallel to the *ac* crystallographic plane when crystallization water molecules are released. The presence of direct hydrogen-bonding interactions between the adjacent layers (Figure 11) precludes further compression. The loss of the coordinated water molecule starts at 80 °C and, as it usually happens, involves a drastic change in the diffraction pattern. The analysis of the XRPD patterns of compound **9** presents some drawbacks due to the preferred orientation of the [100] reflection. Anyway, some interesting information can be inferred. In the crystal structure, 2-D [Cu(pz23dc)(imd)] layers pile up one above the other along the *a* axis and are held together only by means of nondirect hydrogen-bonding interactions established through the water molecules. The removal of the first two intersticial water molecules (O2w and O3w) takes place in the range of 35−65 °C. Once the release of these two water molecules has ended, the complex layers can assemble as puzzle pieces, implying a significant compression of the interlayer space and, therefore, a shifting of the main reflection to greater 2θ values ($T = 75$ °C, $\Delta 2\theta = 1.316°$, $\Delta d = 1.174$ Å). Thereafter, the third water molecule (O1w) is occluded in the crystal structure and comes out at greater temperatures (100 °C), causing a noticeable change in the XRPD pattern. Finally, upon exposure of the dehydrated products **6**, **8**, and **9** to air at room temperature for 24 h, they changed back to the initial hydrated form, retaining the crystallinity which supports the occurrence of a reversible dehydration process.

Magnetic Properties. All compounds, except **4**, show a decrease of the $\chi_M T$ value with the lowering of the temperature, indicating an overall antiferromagnetic behavior. The $\chi_M T$ curve of compound **4** increases continuously at low temperatures upon cooling. This trend is indicative of the predominance of ferromagnetic interactions. Taking into account the structural features of the complexes, their magnetic data have been fitted to the appropriate magnetic model. The model used for each compound and the best fit values are shown in Table 3.

The magnetic interactions between the paramagnetic centers in *pz25dc*-bridged complexes takes place mainly through the pyrazine ring.[9] The magnetic coupling through the pyrazine bridge has in almost all cases an antiferromagnetic character. Nonetheless, in compound **4** and in a compound based on the μ-pyrazine-2,3-dicarboxylato-k^2N,O:N′,O′ ligand, ferromagnetic interactions through the pyrazine ring prevail.[4a] This behavior is explained by the accidental orthogonality between the magnetic orbitals (a $d_{x^2-y^2}$ type

(41) Henry, M.; Taulelle, F.; Loiseau, T.; Beitone, L.; Férey, G. *Chem.—Eur. J.* **2004**, *10*, 1366−1372.

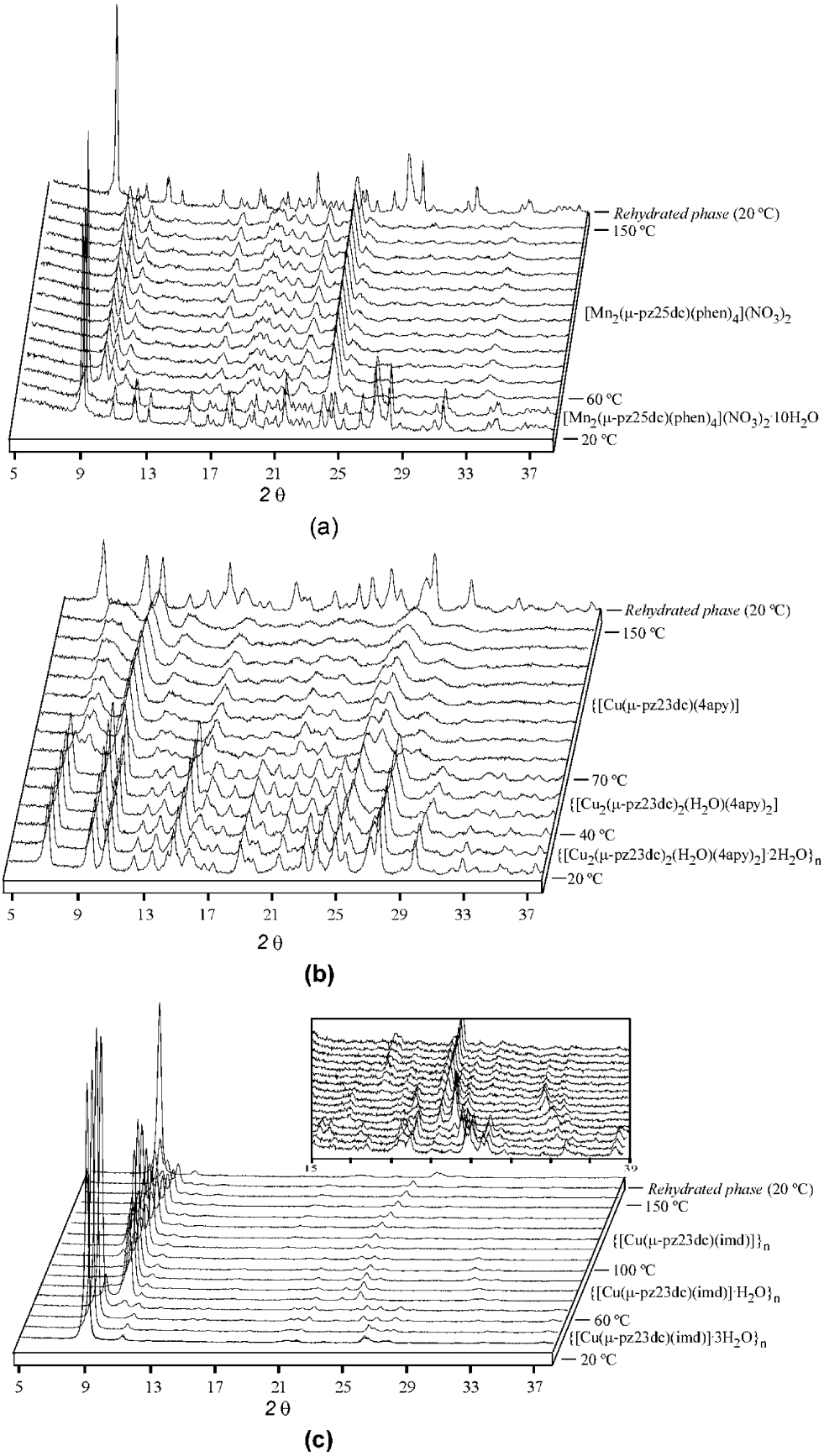

Figure 13. Variable-temperature XRPD patterns of compounds **6** (a), **8** (b), and **9** (c). In all cases, the last one was collected 24 h after cooling and belongs to the rehydrated product.

Table 3. Best-Fit Values for Compounds **1**, **2**, **4**−**9**

M(II)	compound	J (cm^{-1})	g	$R \times 10^5$	n^2J	model
Mn	**1**	−0.16	2.00	21	−4.00	chain[42]
Fe	**2**	−0.58	2.10	11	−9.28	chain[42]
Cu	**4**	+0.04	2.11	0.27	+0.04	chain[43]
Cu	**5**	−0.88	2.10	0.93	−0.88	chain[44]
Mn	**6**	−0.26	2.00	8	−6.50	dimer[4]
Cu	**7**	−0.18	2.13	0.15	−0.18	chain[44]
Cu	**8**	−5.31	2.16	0.12	−5.31	dimer + monomer[45]
Cu	**9**	−2.50	2.16	0.11	−2.50	dimer[46]

orbital in square pyramidal or elongated octahedral geometries) of copper(II) atoms. One of the metals is axially bonded to an endocyclic nitrogen of the pyrazine bridge, while the second metal is equatorially coordinated to the bridging ligand (axial−equatorial coordination mode), leading to a negligible or even zero overlap (accidental orthogonality) between the cited magnetic orbitals and, therefore, allowing the occurrence of a weak ferromagnetism.

On the other hand, copper(II) complexes with axial−axial or equatorial−equatorial coordination modes show antiferromagnetic behavior. Nevertheless, these interactions are mostly weak or very weak because of the extension of the bridging ligand. In this kind of complex, the values of the J magnetic coupling constant usually range between −0.2 and −4 cm^{-1}.[47,48] We have observed that complexes that show an axial−axial disposition of the magnetic orbitals through the pyrazine ring have the lowest values of J, ranging between −0.2 and −0.5 cm^{-1}. On the contrary, an equatorial−equatorial disposition results in a more effective overlap of the orbitals, leading to slightly greater values of J ranging from −0.8 to −4 cm^{-1}. The magnetic coupling constant obtained for compound **5** lies within the last values. These weak values are due to the long σ exchange pathway through the pyrazine ring. Nonetheless, there is a handful of equatorial−equatorial *pyz*-bridged copper(II) complexes which present unusually high antiferromagnetic interactions[49] attributable to a $d\sigma-p\pi$ type interaction between the $d_{x^2-y^2}$ magnetic orbital and pyrazine p_z orbitals. This interaction is allowed by the high displacement of the metal atom from the mean plane of the pyrazine or the high distortion of the pyrazine ring that these compounds show.[9] The involvement of the pyrazine π pathway promotes a strengthening of the antiferromagnetic interaction as predicted by the polarization mechanism.

The π pathway through the pyrazine ring is also involved in the magnetic exchange when t_{2g} unpaired electrons are present. The comparison of the J values of compounds **1**, **2**, **5**, and **6** provides evidence for this. Because different numbers of magnetic orbitals are present in this family, it is more appropriate to compare the values of n^2J instead of those of J (n being the number of magnetic orbitals).[50,51] The n^2J values for compounds **1** ($5^2J = -4.00$ cm^{-1}), **2** ($4^2J = -9.31$ cm^{-1}), and **6** ($5^2J = -6.50$ cm^{-1}) are substantially larger than that for compound **5** ($J = -0.88$ cm^{-1}). The observed order of J values is inconsistent with the M−N bond length, because shorter bond lengths bring about stronger interactions in general. This trend can be explained by the occurrence of $d\pi-p\pi$ interactions between the magnetic orbitals with π-type symmetry around the M−N bonding and the p_z orbitals of the pyrazine ring, which would enhance the magnitude of the magnetic interaction. In fact, for e_g and t_{2g} magnetic orbitals, the pyrazine ring provides the $d_\sigma-PYZ_\sigma-d_\sigma$ and $d_\pi-PYZ_\pi-d_\pi$ main exchange pathways, respectively. For a pyrazine bridge, both pathways lead to antiferromagnetic interactions, as occurs in the antiferromagnetic compounds $[Cu_2(\mu\text{-pyz})(tren)_2](BPh_4)_4$ (σ pathway) and $[(VO)_2(\mu\text{-pyz})(hfac)_2]$ (π pathway).[52] So, for paramagnetic centers such as Mn(II) and Fe(II), we can distinguish $J(e_g-e_g)$ and $J(t_{2g}-t_{2g})$ antiferromagnetic terms and the $J(e_g-t_{2g})$ ferromagnetic term. However, from all of these terms, only those involving the σ and π pathways have a significant strength. As a consequence, the presence of unpaired electrons in t_{2g} orbitals leads to an enhancement of the antiferromagnetic coupling ($n^2J \approx J_\sigma + J_\pi$) compared with those of only e_g unpaired electrons ($n^2J \approx J_\sigma$). Similar behavior has been observed for pyrimidine-bridged metal complexes but with the opposite trend (see the Supporting Information).[51]

In the *pz23dc*-bridged compounds (**7**−**9**), this ligand does not adopt a bis-bidentate coordination mode, and thus, the magnetic properties of these compounds are not related to the direct magnetic interaction through the pyrazine ring. In compound **7**, the magnetic interaction takes place through an extended pathway involving the aromatic ring and the

(42) Fisher, M. E. *Am. J. Phys.* **1964**, *32*, 343−346.
(43) Baker, G. A.; Rushbrooke, G. S. *Phys. Rev.* **1964**, *135*, 1272−1277.
(44) (a) Hall, J. W. Ph.D. Dissertation, University of North Carolina, Chapel Hill, NC, 1977. (b) Bonner, J.; Fisher, M. E. *Phys. Rev. A: At., Mol., Opt. Phys.* **1964**, *135*, 640−658.
(45) Julve, M.; Faus, J.; Verdaguer, M.; Gleizes, A. *J. Am. Chem. Soc.* **1984**, *106*, 8306−8308.
(46) Bleaney, B.; Bowers, K. D. *Proc. R. Soc. London, Ser. A* **1952**, *266*, 95.
(47) (a) Kwiatkowski, E.; Romanowski, G.; Nowicki, W.; Suwinska, K. *Polyhedron* **2001**, *20*, 1097−1100. (b) Sletten, J.; Bjorsvik, O. *Acta Chem. Scand.* **1998**, *52*, 770−777. (c) Grove, H.; Sletten, J.; Julve, M.; Lloret, F. *J. Chem. Soc., Dalton Trans.* **2001**, 1029−1034.
(48) (a) Grove, H.; Sletten, J.; Julve, M.; Lloret, F. *J. Chem. Soc., Dalton Trans.* **2000**, 515−522. (b) Oshio, H.; Nagashima, U. *Inorg. Chem.* **1990**, *29*, 3321. (c) Okubo, T.; Kondo, M.; Kitagawa, S. *Synth. Met.* **1997**, *85*, 1661−1661. (d) Suárez-Varela, J.; Colacio, E.; Romerosa, A.; Ávila-Rosón, J. C.; Hidalgo, M. A.; Romero, J. *Inorg. Chim. Acta* **1994**, *217*, 39−44.
(49) (a) Graf, M.; Stoeckli-Evans, H.; Escuer, A.; Vicente, R. *Inorg. Chim. Acta* **1997**, *257*, 89−97. (b) Burkholder, E.; Golub, V.; O'Connor, C. J.; Zubieta, J. *Inorg. Chem.* **2003**, *42*, 6729−6740.
(50) Lloret, F., Julve, M.; Cano, J.; De Munno, G. *Mol. Cryst. Liq. Cryst.* **1999**, *334*, 569−585.
(51) Ishida, T.; Kawakami, T.; Mitsubori, S.; Nogami, T.; Yamaguchi, K.; Iwamura, H. *J. Chem. Soc., Dalton Trans.* **2002**, 3177−3186.
(52) Haddad, M. S.; Hendrickson, D. N.; David, N.; Cannady, J. P.; Drago, R. S.; Bieksza, D. S. *J. Am. Chem. Soc.* **1979**, *101*, 898−906.

carboxylate group and leads to an almost negligible magnetic interaction ($J = -0.18$ cm^{-1}). A similar J (-0.25 cm^{-1}) value has been reported for compound [Cu(pz23dc)$(H_2O)_2$]·H_2O with the same coordination mode of the *pz23dc* ligand.[6b] The analysis of the magnetic data of compounds **8** and **9** by fitting to a magnetic model is more tricky because in both compounds we can distinguish two different exchange pathways. The first one involves the same long pathway found in compound **7**, and the second one occurs through the μ-oxo bridge. A magnetic model which could take into account the two coupling constants, as far as we know, has not been previously reported, but assuming that the extended pathway through the *pz23dc* ligand leads to negligible interactions as observed in compound **7**, we can interpret the magnetic data, as a first approximation, to μ-oxo-bridged copper(II) dimers[53] in compound **9** and copper(II) dimers together with isolated Cu(II) monomers for compound **8**. The fit reproduces well the magnetic curves, and the obtained J and g values are listed in Table 3.

The studies involving Cu(II) ions bridged by a double μ-oxo bridge in a parallel-planar geometry have reported that weak ferro- and antiferromagnetic interactions are observed (values of J ranging from -4.30 to $+1.26$ cm^{-1}).[54] These magnetostructural studies have shown that the nature and magnitude of the magnetic coupling between the parallel magnetic orbitals depends on the values of the angle at the bridge ϕ and the out-of-plane Cu···O bond distance (R_0). Values of $\phi = 96.30°$ and $R_0 = 2.498$ Å in **8** and $\phi = 102.17°$ and $R_0 = 2.467$ Å in **9** are in good agreement with the observed antiferromagnetic behavior.

Acknowledgment. This work was supported by the Spanish Ministerio de Educación y Ciencia (MAT2005-03047) and the Universidad del País Vasco/Euskal Herriko Unibertsitatea (9/UPV 00169.310-15329/2003). G.B. thanks the Eusko Jaurlaritza/Gobierno Vasco for a doctoral fellowship (BF102.79).

Supporting Information Available: Final Rietveld refinement plots of compounds **2** and **3**. Hydrogen bonding and $\pi-\pi$ interaction data. Coordination modes of the *pz23dc* ligand. Thermogravimetric curves (TG/DTA) of compounds **6**, **8**, and **9**. $\chi_M T$ versus T plots of compounds **1**, **2**, and **4**−**9**. Magnetic coupling constant trends in pyrazine- and pyrimidine-bridged complexes. X-ray crystallographic files in CIF format. This material is available free of charge via the Internet at http://pubs.acs.org.

IC060221R

(53) Myers, B. E.; Berger, L.; Friedberg, S. *J. Appl. Phys.* **1969**, *40*, 1149−1151.

(54) (a) Chiari, B.; Helms, J. H.; Piovesana, O.; Tarantelli, T.; Zanazzi, P. F. *Inorg. Chem.* **1986**, *25*, 2408−2013. (b) Greenaway, A. M.; O'Connor, J. C.; Overman, J. W.; Sinn, E. *Inorg. Chem.* **1981**, *20*, 1508−1513. (c) Pasini, A.; Demartin, F.; Piovesana, O.; Chiari, B.; Cinti, A.; Crispu, O. *J. Chem. Soc., Dalton Trans.* **2000**, 3467−3472. (d) Escribá, E.; Server-Carrió, J.; Lezama, L.; Folgado, J. V.; Pizarro, J. L.; Ballesteros, R.; Abarca, B. *J. Chem. Soc., Dalton Trans.* **1997**, 2033−2038.